CONF-780508--61

LA-UR -78-1627

TITLE: INERTIAL CONFINEMENT FUSION REACTOR CAVITY PHENOMENA

AUTHOR(S): I. O. Bohachevsky, J. F. Hafer, J. J. Devaney, and J. H. Pendergrass (all L-5)

SUBMITTED TO: Proc. 3rd ANS Topical Meeting on the Technology of Controlled Nuclear Fusion (May 1978), Santa Fe, NM

MASTER

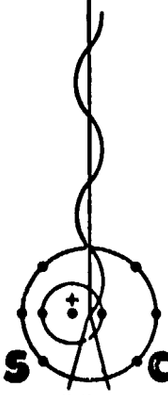

los alamos
scientific laboratory
of the University of California
LOS ALAMOS, NEW MEXICO 87545

An Affirmative Action/Equal Opportunity Employer

Form No. 836
St. No. 2629
1/75

UNITED STATES
ENERGY RESEARCH AND
DEVELOPMENT ADMINISTRATION
CONTRACT W-7405-ENG. 36

INERTIAL CONFINEMENT FUSION REACTOR CAVITY PHENOMENA

I. O. Bohachevsky, J. J. Devaney, J. F. Hafer, and J. H. Pendergrass

Los Alamos Scientific Laboratory
Los Alamos, New Mexico 87545

ABSTRACT

Cavity phenomena in Inertial Confinement Fusion (ICF) are created by the interaction of energy released by the fuel pellet microexplosion with the medium inside the reactor cavity. The ambient state of the medium in ICF reactor cavities is restricted primarily by its effects on laser beam propagation and on the fuel pellet trajectory. Therefore, a relatively wide choice of ambient conditions can be exploited to gain first-wall protection and advantages in energy extraction. Depending on the choice of ambient cavity conditions and on fuel pellet design, a variety of physical phenomena may develop and dominate the ICF reactor cavity design. Because of the cavity phenomena, the forms of energy released by the fuel-pellet microexplosion are modified before reaching the first wall, thus giving rise to different cavity design problems. The types of cavity phenomena encountered in the conceptual design of ICF reactors are examined, the approaches available for their modeling and analysis are discussed, and some results are presented. Most phenomena are sufficiently well understood to permit valid engineering assessments of the proposed ICF reactor concepts.

INTRODUCTION

In Inertial Confinement Fusion (ICF) the implosion and burn of a D-T fuel pellet are independent of the initial (ambient) cavity conditions, This aspect of ICF is different from that of magnetically confined fusion in which compression, heating, and ignition of the DT plasma cannnot be separated from the ambient conditions inside the confinement vessel. Thus the requirement for unobstructed transmission of the driver-beam energy through the cavity medium to the fuel pellet is the dominant constraint on ICF cavity conditions between microexplosions. This freedom in the selection of ambient conditions is exploited to gain first-wall protection and advantages in energy extraction (e.g., making use of MHD generators).

Cavity phenomena develop from the interaction of the energy released by the fuel-pellet microexplosion with the ambient medium in the reactor cavity. They modify the energy release forms and thus give rise to different cavity first-wall design problems. Therefore, the cavity phenomena must be identified and analyzed before the first-wall design problems can be specified and solved. Consequently, the objectives of modeling and investigating the cavity phenomena are:

1. Determine transient thermal and mechanical wall loadings,
2. estimate the damage to the cavity first wall and structure caused by neutrons, x rays, and pellet debris; and
3. determine the requirements for restoration of favorable cavity conditions between successive fuel-pellet microexplosions for repetitive operation.

For each particular ICF reactor design the relevant and dominant physical phenomena are deter-

Work performed under the auspices of US DOE.

mined by the first-wall protection concept and by the ambient cavity conditions. We will summarize and illustrate the general classes of physical phenomena that require modeling and study in the conceptual ICF reactor design stages and outline current research at LASL.

ICF REACTOR CAVITY CONCEPTS, AMBIENT CONDITIONS, AND CAVITY PHENOMENA

ICF reactor cavity concepts, proposed in the past, may be grouped into two generic classes:

1. Cavities with permanent solid walls; their lifetime may be extended by protecting the walls with sacrificial liners or magnetic fields; and
2. Cavities with renewable fluid walls exemplified by the wetted or thick-curtain walls.

The concept in which the cavity is filled with a protective gas may belong to either class: if the gas is totally replaced after each microexplosion then it can be viewed as a renewable wall, however, if the gas content is only partially replaced, then its pressure and density may be viewed as ambient conditions in a cavity with solid walls. This example illustrates that it is not always possible to differenciate unambiguously between the cavity phenomena and the first-wall problems.

Ambient cavity conditions for ICF reactors may be divided into three broad classes:

1. Vacuum, i.e., the mean free path of a pellet-debris ion is longer than or comparable to the cavity size for both momentum and charge-exchange encounters;
2. Background fluid medium (which may be partially ionized by the initial burst of radiation from the pellet), in which debris-ion mean free paths are short for at least one kind of encounter;
3. Mixture of vapor and liquid phases.

Not all these ambient conditions and first-wall protection schemes are compatible. A high vacuum can be maintained only in cavities with solid walls; therefore, this choice is available only for cavity concepts employing bare refractory metal walls, sacrificial liners, or magnetic-field wall protection. A protective gas may be introduced into the cavity to attenuate the x rays transmitted to the walls and to slow down the fast pellet debris ions. The density of such a protective atmosphere will be limited by its effects on the trajectories of injected fuel pellet and on the transmission characteristics of the laser beam . The buffer gas may be used with or without magnetic-field wall protection. Vapor and liquid phases will be present in the cavity when liquid lithium is used for wall protection either as an adhering thin film or as a free-falling thick curtain wall.

Depending on the choice of ambient cavity conditions and fuel-pellet design, the following cavity phenomena may dominate the reactor cavity design:

1. Unaffected energy transmission (in the form of neutrons, x rays, and debris ions) from the exploded pellet to the cavity wall;
2. Debris ion expansion in the presence of a magnetic field;
3. Debris ion expansion through a background medium, whether in the presence of a magnetic field or not, with average ion mean free path short relative to any cavity dimension for at least one type of encounter;
4. large-scale (blast or acoustic wave) and small-scale (turbulence) motions of the buffer gas with and/or without radiation or magnetic-field effects;
5. hydrodynamic wave motion with evaporation and condensation phenomena;

We at LASL recognized early the importance of reactor cavity phenomena in modeling ICF reactor concepts, and initiated numerous studies in this area. Results of these studies are presented below, together with an indication of the ongoing investigations.

UNAFFECTED FUEL PELLET ENERGY TRANSMISSION

The modeling of the free expansion of energy forms released by the fuel-pellet microexplosion (neutrons, x rays, energetic ions) leads to the analysis of the interaction of each energy form with the solid or liquid first wall. Neutrons generated during D-T fusion pass through the inner cavity wall with negligible energy loss and damage the material through atomic displacements and related effects. These effects are not considered

cavity phenomena in this paper and therefore are not discussed further. We will, however, discuss in some detail the three effects caused at the wall by both x rays and energetic ions: impulse, surface temperature increase, and cause material loss.

The impulse, p_T, delivered to the first wall by the kinetic energy of the fast debris ions is given by:[1]

$$p_T = \frac{\sqrt{fYM}}{2\sqrt{2}\,\pi R^2},$$

where Y is the fuel-pellet energy yield, f is the fraction of yield in debris ions, M is the pellet mass, and R the cavity radius.

The impulse generated at the surface of the wall by ablation resulting from x-ray or debris-ion energy deposition is:[1]

$$p_T = \frac{\eta_x Y}{4\,R^2\pi\sqrt{2H}},$$

where x is the fraction of yield in x rays, H is the heat of evaporation of the wall material, and η is the fraction of the maximum attainable blowoff velocity representing the mean vapor motion.

The second problem is that of surface temperature increase. The model and the analysis of the thermal response of the wall to pulsed energy deposition have been described previously;[2,3] the results, however, are too extensive to be included here.

The third problem is that of wall material loss through mechanical erosion by ion sputtering and thermal evaporation from x-ray and ion debris heating.

The determination of the mechanical sputtering erosion has been described in detail in two reports by Bohachevsky and Hafer.[4,5] Results, illustrated in Fig. 1, show the calculated amount of wall material eroded per gram of pellet material as a function of debris ion energy. The loss of material due to evaporation from first-wall inner surfaces induced by x-ray and charged-particle energy depositions has been modeled analytically and numerically.[5]

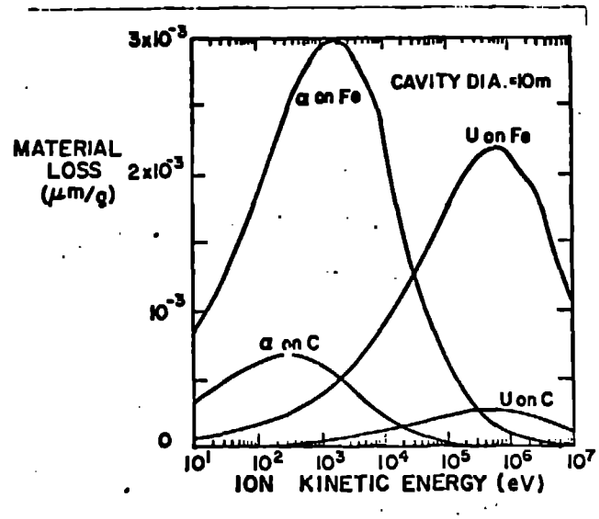

FIGURE 1 Sputtering erosion of wall material.

The analytical model is restricted to constant physical properties but includes arbitrary surface energy fluxes on the inner and outer surfaces, as well as thermal radiation fluxes at the inner surfaces and a constant temperature at the outer surface. It was used primarily to verify the model calculations.

The numerical model removes the principal restriction of the analytical models - constant thermophysical material properties - and is presently most heavily utilized. It is one-dimensional, but includes an arbitrary number of slabs and radiating surfaces. The thermal conductivity and heat capacity of the wall material are approximated by polynomial functions of temperature. The initial and boundary temperatures and the energy-deposition profile and history can be prescribed arbitrarily.

The rate of evaporation as a function of surface temperature is computed using the Langmuir theory, with an arbitrary sticking coefficient, and vapor pressure represented by the usual Arrhenius-type expression. Multicomponent evaporation is determined by weighting the evaporation rates of individual specie by their mole fractions in the surface layers. Self-shielding of the first wall by the evaporated material is taken into account by treating the evaporated material as an equivalent thickness of the condensed phase.

The amount of surface material evaporated from the first wall surface by a pellet microexplosion depends on the integral over the pulse duration of the vapor pressure of the wall material divided by the square-root of the surface temperature; and because the vapor pressure is proportional to the inverse exponential function of the instantaneous value of the surface temperature, the amount of material lost by evaporation is completely determined by the surface-temperature history. Of course, this history depends on many parameters that characterize the pellet energy output and wall material properties; the details of these dependencies may be found, for example, in Refs: (2), (3), and (6).

Studies of first-wall evaporation indicate that the most important characteristic, apparently, is the energy spectrum of the incident radiation. More energetic radiation penetrates deeper and deposits its energy in a larger volume, inducing a lower surface-temperature increase,[2] whereas the opposite is true for less energetic (softer) spectra. However, for less penetrating radiation, a smaller amount of evaporated material is sufficient to prevent further signficant radiation-energy transport to the solid surface because of the self-shielding effect. Therefore, it is difficult to predict the trend in each particular case without detailed calculations. This is illustrated in Fig. 2, showing the amount of material evaporated from an ATJ graphite surface by an x-ray pulse as a function of photon energy. When 2 J/cm^2 are deposited in 10^{-4} s, the effect of self-shielding at low energies (decreasing material loss with decreasing energy) is evident; however, when 4 J/cm^2 are deposited in 10^{-3} s, the self-shielding mechanism is not effective. Because photon penetration increases with increasing energy and induces a lower surface-temperature rise,[2] all curves in Fig. 2 show a dramatic decrease in evaporation with increasing energy. The steepness of the decrease is a consequence of the inverse exponential dependence of the evaporation rate on surface temperature.

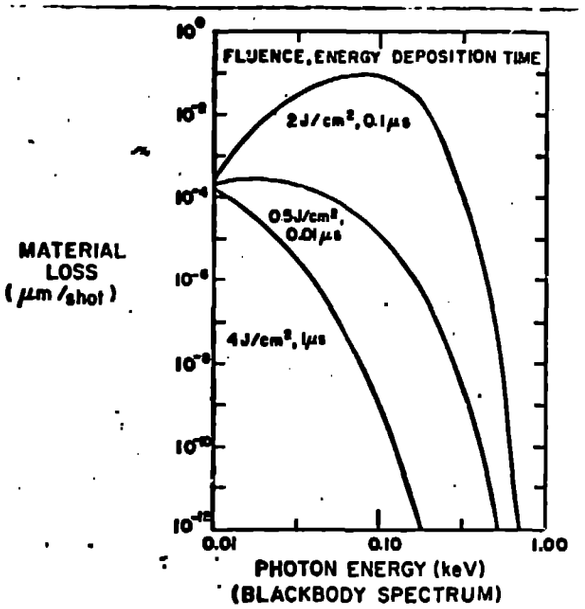

FIGURE 2 Surface evaporation.

Pellet Debris Expansion in a Magnetic Field

The problem of modeling debris ion expansion in vacuum with an axial magnetic field arises in the analysis of the magnetically protected reactor cavity concept.[7] The modeling has been successfully accomplished with the computer code LIFE; details of the computational method and results have been presented previously.[8] Here we include only sample results. The ion distribution at different times during expansion, and the number and energy distribution of particles incident on the walls of the cavity are illustrated in Figs. 3 and 4, respectively.

The x rays do not interact with the magnetic field, and therefore their effects are determined as in the previous case. The material loss through mechanical erosion occurs only on specially designed parts of the wall known as energy sinks. They have been modeled and analyzed extensively.[4]

Pellet Debris Ion Expansion Through a Background Gas and Magnetic Field

A background gas may be added to the magnetically protected cavity to shield the cylindrical walls from x-ray heating and thus retard the wall

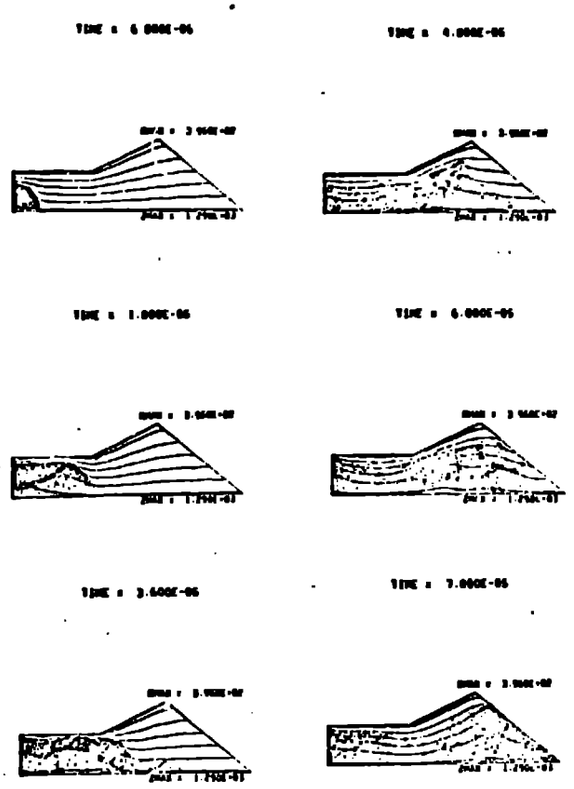

FIGURE 3 Debris ion expansion in a cylindrical magnetic field; time in seconds, dimensions in centimeters.

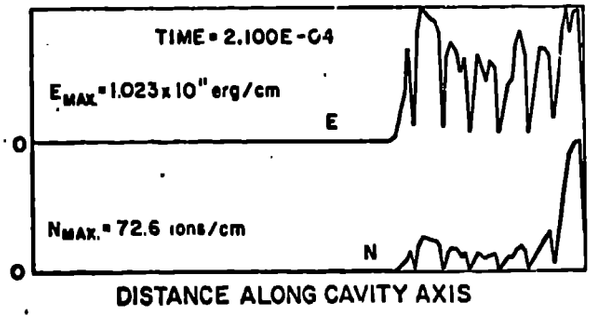

FIGURE 4 Cumulative energy (E) and ion (N) depositions in the cavity wall.

evaporation. The analysis of such a cavity concept requires modeling of ion motion in a cylinder filled with a partially ionized fluid medium and an imposed axial magnetic field. Ionization occurs primarily as a consequence of the burst of radiation from the exploding fuel pellet; its level is assumed to be high enough to make the plasma a good conductor. The fuel pellet ions created in the microexplosion interact with the background fluid through the action of the magnetic field and through charge exchange.

The physical model therefore must include two components: the background fluid and the debris ions. The behavior of the background fluid is described by the Lundquist equations supplemented by an appropriate equation of state and a rate equation to describe the changes in the degree of ionization. The debris ion motion is determined by statistical modeling (PIC), with rate equations describing the average ion charge state. Individual ion trajectories are determined by integrating the equation of motion for each simulation ion, with the Lorentz force providing the acceleration. The background fluid motion and the ion motion are coupled through Maxwell's equations in which the displacement current has been neglected. Appropriate reaction rates are included to describe the changes in the average ion charge and in the degree of ionization of the background medium.

We have formulated the mathematical description of this model with a method of solution, and are coding the program for its calculation. In this program, the Lundquist equations will be solved with a first-order finite-difference scheme expressed in conservation form to facilitate computation with imbedded MHD shocks. Ion motion will be computed, as in the LIFE code, from conservation of canonical momentum and from time integration employing cell-area weighting. The code can distinguish 50 different ion species. The capacity of the currently available CRAY-I computer will allow parametric studies with this model.

Effects of a Protective Buffer Gas

A protective fluid medium may be used in a cavity with or without a magnetic field. Without a magnetic field it will be most effective if the combination of density and cavity size can significantly attenuate low-energy x rays and appreciably slow down the energetic pellet-debris ions, as proposed by Conn and collaborators.[3] Some effects of the protective atmosphere and restrictions on its characteristics will be discussed in this section.

When the density is sufficiently high to absorb the x rays and dissipate the debris ion energy, then the mean free path is sufficiently short and a blast wave will develop after the pellet microexplosion. However, the difference between the pellet and background densities is sufficiently large as to cast doubt on the validity of similarity-solution representations of the blast wave within the confines of the reactor cavity. (In obtaining similarity solutions of the microexplosion phenomenon it is assumed that the initial pellet mass is negligible in comparison to the mass of the fluid swept by the blast wave; clearly, this assumption is not valid when the fuel pellet mass is comparable to the mass of the fluid contained in the cavity.) To investigate the validity of blast-wave similarity solutions and to obtain representations valid for all pellet masses, Freiwald and Axford[9] modified the classical Taylor-Sedov similarity solution to account for nonnegligible pellet mass. The results predicted by their theory are shown in Figs. 5 and 6. As intended, the Freiwald-Axford solution removes the singularity of the Taylor-Sedov solution at the origin and, instead, pre-

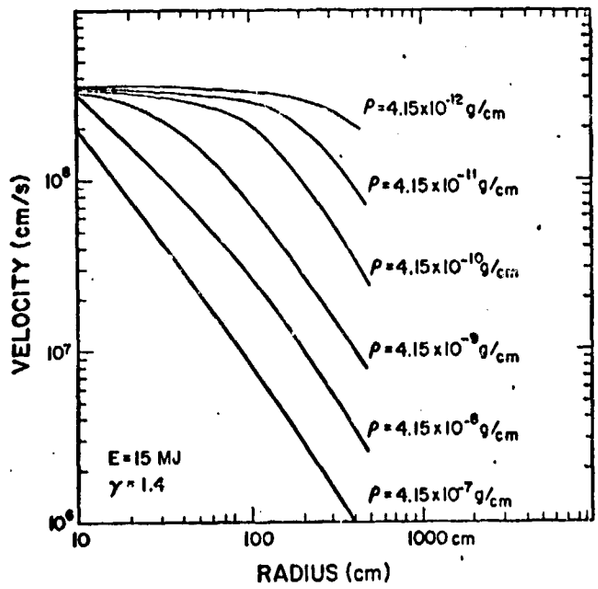

FIGURE 5 Gas expansion velocity predicted by Freiwald-Axford[8] blast wave analysis.

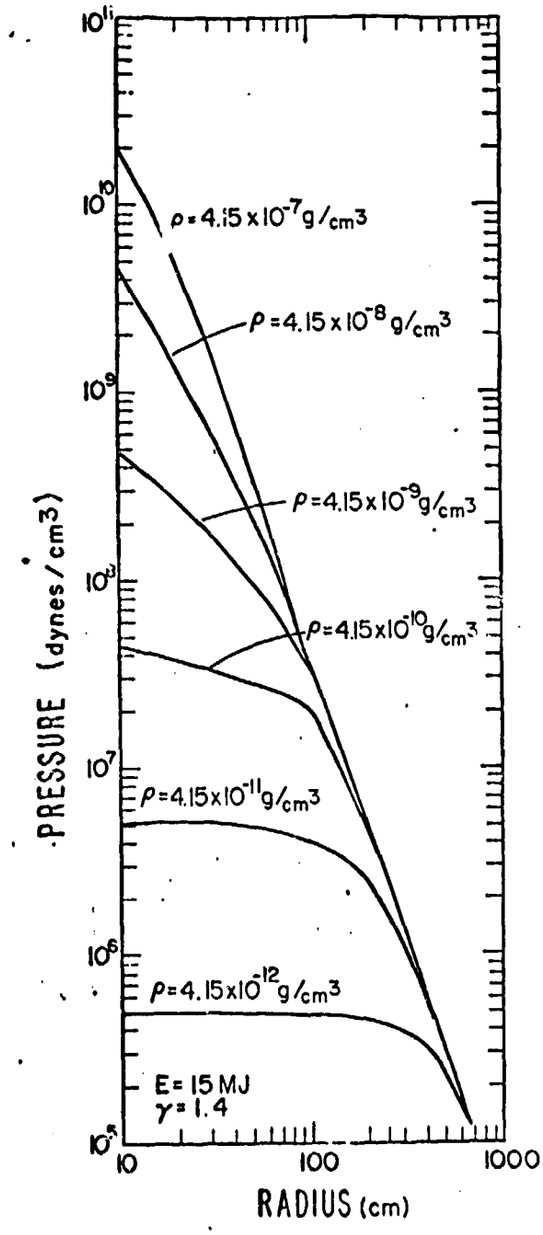

FIGURE 6 Pressure predicted by Freiwald-Axford[8] blast wave analysis.

TRIM SIZE: 8½" x 11"
REDUCED IMAGE SIZE: 7" x 9" PLUS FOLIO = 7" x 9½"
MARGINS: HEAD 2⅛, BIND 2"
SHOOT AT 60%
FORMAT NO. 2

dicts for small radii a velocity about equal to the free expansion velocity; this result appears physically plausible. For large radii (>10 m) and conditions at which the calculations reported in Ref. (9) were carried out, Freiwald and Axford predict velocities about half as high as those predicted by the Taylor-Sedov solution, and the pressure predictions disagree by an equally large factor. These differences suggest that simple similarity solutions cannot always be used to accurately predict the development of a blast wave in the reactor cavity.

The Freiwald-Axford analysis is a significant improvement over the Taylor-Sedov similarity solution, but, it does not include the effects of radiation; in cases when the buffer gas in the cavity is sufficiently opaque to absorb the x rays emitted during pellet microexplosion, the radiation-energy transport should be included in the determination of fireball formation and blast-wave development. Although much has been accomplished in this area in connection with the analysis of weapons effects, adequate modeling of these phenomena for the set of conditions anticipated in ICF reactor cavities has not yet been attempted.

Following their formation, blast waves in a spherical cavity will be reflected back and forth between the wall and the cavity center. The number of reflections in between successive pellet microexplosions may be estimated crudely by using the acoustic approximation:

$$N = \frac{a}{pps \cdot R} ,$$

where a is the sound speed and pps denotes number of pulses per second. At a pressure of 1 torr and a density of 3.33×10^{-7} g/cm^3, when the effective adiabatic exponent equals 1.4, the sound speed equals 75×10^3 cm/s; therefore, 15 successive wave reflections will occur in a 5-m radius cavity operating at 10 pps. Thus, attenuation of ~ 7% per reflection may be required to dampen the wave motion to insignificant amplitude between successive pellet injections. Numerical modeling and analysis of similar problems indicate that damping of such magnitude will be generally present.

In addition to large-scale wave motion, one encounters small-scale turbulence in the cavity, resulting from nonuniform wave reflections induced by cavity wall openings and protrusions (for, e.g., optics, pellet injection, gas circulation) and by the pumping required to circulate cavity gas. The effect of medium inhomogeneities on the injected pellet trajectory may be estimated by integrating the fluctuating aerodynamic drag and pressure forces over the length of the trajectory. The resulting expression for the perturbation of the intended pellet position, δr, is:

$$\delta r = \frac{\pi r_p^2}{m} \int_R^0 \int_R^r C_D \rho \left(\frac{\delta v}{v} + \frac{1}{2} \frac{\delta \rho}{\rho} + \frac{\delta p}{C_D \rho v^2} \right) dr' dr ,$$

where r_p is the pellet radius, m the pellet mass, C_D the drag coefficient, ρ the cavity gas density, p the pressure, v the pellet velocity relative to the gas, and δ denotes the fluctuation of the quantity following it. This expression is valid in a regime in which the drag force is proportional to the square of the velocity and the pressure fluctuations occur over a distance approximately equal to r_p. A corresponding expression can be easily derived for conditions that require other assumptions. The expression for δr obtained above estimates the departure from the intended position along the trajectory of the pellet (equivalent to the delay $\delta r/v$ in pellet arrival time); a corresponding expression for transverse perturbation involves pressure nonuniformity only and can be derived without difficulty.

If the medium fluctuations cannot be kept within limitations set by the above expression for δr then it will be necessary to track each pellet in flight and aim all laser beams accordingly. This procedure, however, will not be effective if fluc-

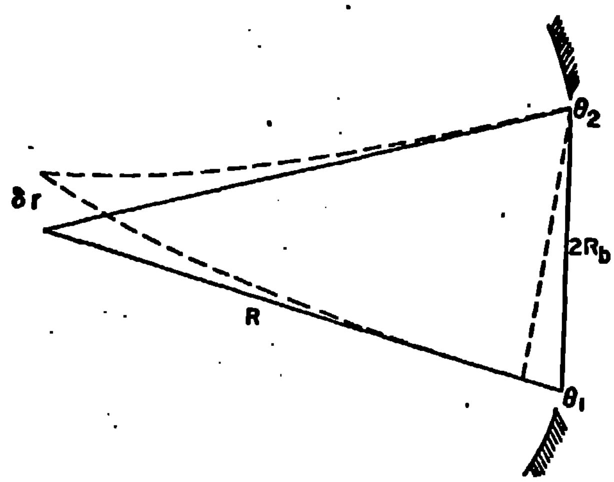

FIGURE 7 Effect of cavity medium inhomogeneity on the beam path.

tuations in the index of refraction caused by density inhomogeneities in the medium are sufficiently severe to displace the focal point of the beam appreciably. The lateral displacement of the beam focus (assuming ideal focusing can be attained; comments about this assumption will be made below) is easily determined by calculating the optical path length along two rays separated initially by the beam diameter $2R_b$ as indicated schematically in Fig. 7. The result for the lateral displacement of the focus is:

$$\delta r = \frac{R}{2R_b} \left\{ \int_{R,\theta_1}^{0,\theta_1} (n-1) \frac{\delta\rho}{\rho} dr - \int_{R,\theta_2}^{0,\theta_2} (n-1) \frac{\delta\rho}{\rho} dr \right\}$$

where n is the index of refraction and the integrations are carried out along the two rays θ_1 and θ_2. The above relation may express the most restrictive condition on the homogeneity of the cavity medium; most likely it will have to be verified experimentally.

In addition to the effects induced by inhomogeneities in the cavity buffer gas, the laser beam will be affected by self-generated processes. The wide range of light intensities encountered in propagation of focused laser beams in large gas-filled cavities gives rise to a multitude of competing processes that affect the delivery of light energy onto the fuel pellet. These processes include: multiphoton, tunneling, and cascade ionization; absorption; Rayleigh, Brillouin, and Raman scattering; stimulated Raman scattering; refraction; self-focusing; inverse bremsstrahlung; ion polarization; ponderomotive force; thermal blooming; inverse blooming or trapping; and laser-induced detonation. For proposed commercial reactor cavity parameters some effects will certainly be negligible; however, a comprehensive analysis that would identify the important effects is not yet available.

Henderson[10] obtained results which describe the defocusing of the laser beam due to induced ionization and consequent reduction of the index of refraction, and Conn with his collaborators,[3] utilizing the model and analysis of Hacker, Cohn, and Lax,[11] concluded that laser-induced breakdown will not significantly hinder the delivery of beam energy onto the fuel pellet. As indicated previously, the question whether these are the most important effects, and, if not, what other physical mechanisms should be considered, has not been answered yet.

We wish to mention a problem not usually discussed in the analyses of gas-filled cavities; the heat transfer from the buffer gases to fuel pellets during their travel to the center of the cavity. A simple estimate shows that absorption of all the photon energy emitted during the pellet microexplosion will raise the buffer-gas temperature to several electron volts; this is the reason why, in modeling magnetically protected cavities with a background gas, the degree of ionization must be calculated. During a conservatively short pellet transit time of 10^{-3} s, the high ambient temperature will penetrate to a significant extent, $\sim 3 \times 10^{-2}$ cm, into a pellet material with a typical thermal diffusivity of 0.25 cm^2/s. Such depth may exceed the radii of presently considered fuel pellets. Therefore, unless the gas is entirely replaced between successive microexplosions (which may not be easily accomplished in cavities with

radii of several meters operating at tens of pulses per second), cryogenic pellets will not survive the resulting high-temperature cavity environment in their original state and even the integrity of high-pressure metal-clad microballoons may be suspect.

Cavity Conditions with Phase Transitions

To illustrate the conditions and problems expected in reactor cavities containing, by design, mixtures of liquid and vapor phases, we present in this section results of a numerical computation of the response of a thick lithium curtain wall (as proposed in the lithium-fall reactor concept) to neutron-energy deposition following a pellet microexplosion.

The configuration analyzed incorporates a cylindrical, 50-cm-thick, curtain of flowing lithium--occupying the space between radii of 400 and 450 cm, falling in a normal gravity field with arbitrarily prescribed initial velocity inside a cylindrical cavity of 500 cm radius--and a spherically symmetric neutron source, as shown in Fig. 8. The neutron energy is deposited in the liquid lithium with an exponentially decreasing intensity (e-folding distance, 70 cm) within 10^{-9} s; the total deposited energy is 3000 MJ, and the fraction intercepted by a 1-cm-high cylindrical ring is 3.75 MJ.

The modeling consisted of determining numerically the one-dimensional radial motion in the equatorial plane through the center of the fuel pellet and the superposition of this motion on the uniformly accelerating (under the force of gravity) axial flow. The initial velocity in the vertical direction was 500 cm/s, as indicated in Fig. 8. Thus, the analysis did not include disturbances propagating up and down the lithium curtain.

The radial hydrodynamic motion was determined with the CHART-D code;[12] features of this code relevant to the present calculation are:

- Lagrangean formulation of the hydrodynamic equations of motion with artificial viscosity,
- local thermodynamic equilibrium with radiation energy transport option suppressed,

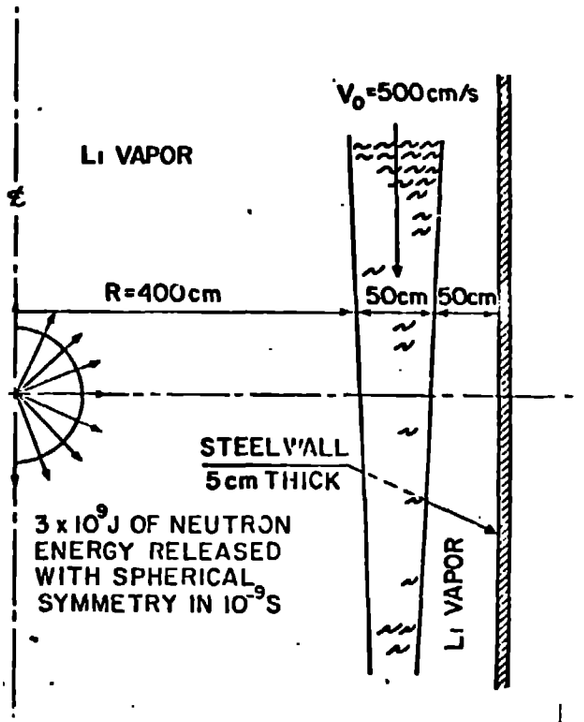

FIGURE 8 Lithium curtain wall model.

- analytic representation of the equation of state with sufficient parameters to accurately approximate phase transitions, the melting curve, and the triple line.

Figures 9 and 10 are a sequence of snapshots depicting the motion of the liquid curtain after the neutron-energy deposition: the curtain splits into two halves and breaks up into spray following reflections at the cylinder axis and from the cylinder wall. The temperature distribution in the curtain and the heating of the central and outer lithium vapor regions (initially at 600K and vapor pressure) after compression by the expanding curtain are shown in the lower half of Fig. 10.

The superposition of radial and axial motions is presented in Fig. 11. This figure shows the trajectories of the centers of mass of the two halves of the curtain (solid lines) and of its inner edge (dashed line) after injection with initial downward velocity of 500 cm/s and after neutron-energy deposition. Gravitational acceleration was included in this calculation. As can be seen,

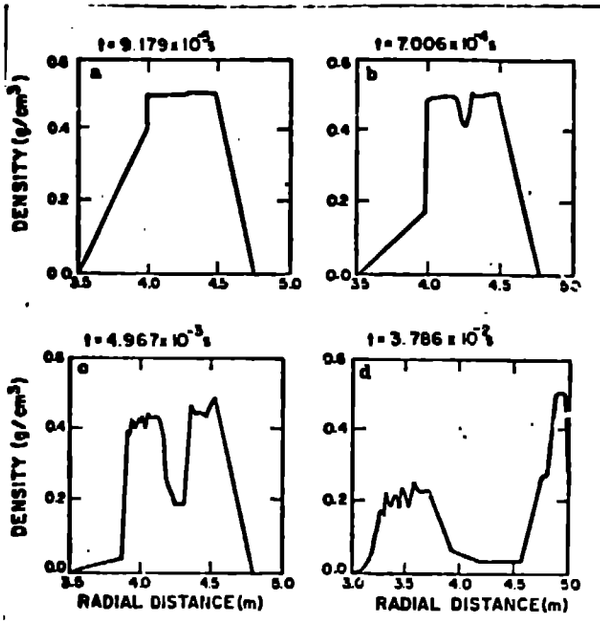

FIGURE 9 Curtain wall density distribution.

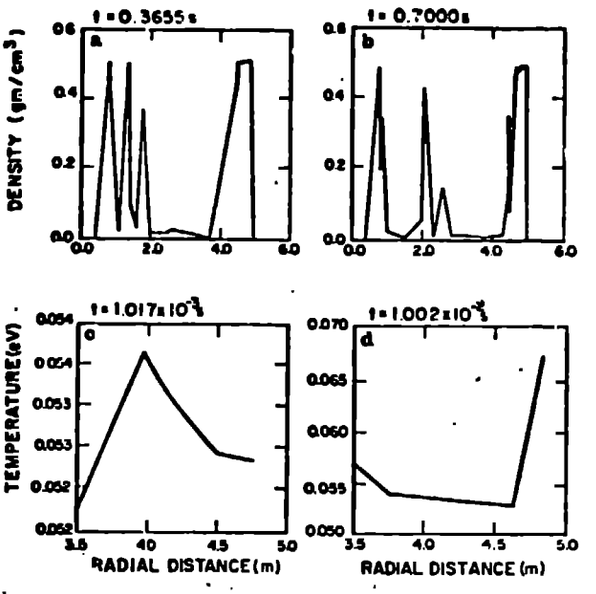

FIGURE 10 Curtain wall density and temperature distributions.

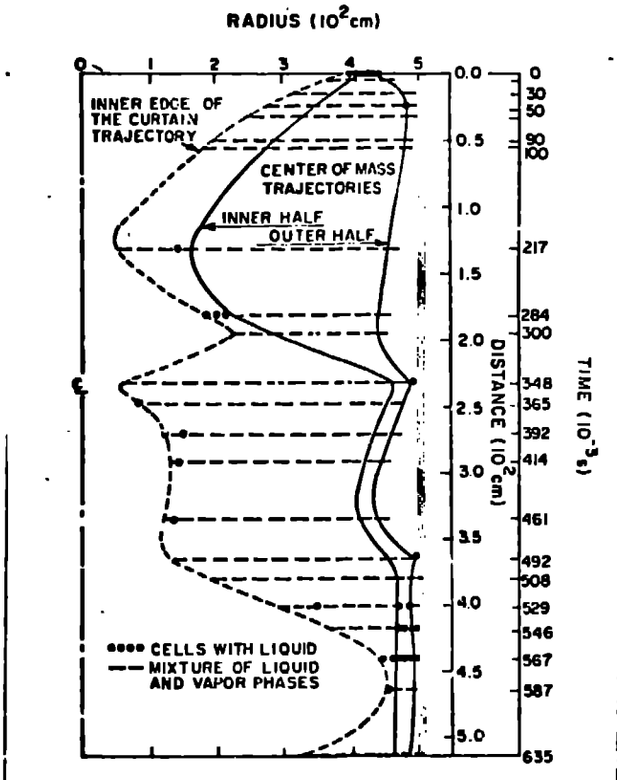

FIGURE 11 Curtain wall motion.

the lithium fills the cavity almost completely for the duration of this calculation, mostly as a mixture of liquid and vapor phases (indicated by horizontal dashed lines) with only a few isolated regions of liquid (indicated by solid circles). Clearly, this spray-like medium must be removed from the cavity before the next pellet can be injected and ignited. The amount of vapor generated will be much larger, and the outward motion of the curtain faster, when the effects of x-ray and debris energy deposition are included in the analysis.

CONCLUDING REMARKS

Our discussion of cavity phenomena relevant in the conceptual design of ICF reactors does not pretend to present a complete and comprehensive analysis of all the phenomena of interest. It only serves as an illustrative selection of problems which, in our opinion, require resolution before credible reactor designs can be proposed. Our choice of problems and approaches to solutions reflect judgments and opinions prevalent in the Systems and Applications Group of the Los Alamos Scientific Laboratory. We feel we have demonstrated that the analysis of ICF reactor cavity phenomena is sufficiently well-advanced to allow a realistic

modeling of the reactor systems and a realistic assessment of the possibilities for the solution of the outstanding problems.

ACKNOWLEDGMENT

Helpful comments and suggestions by T. G. Frank are gratefully acknowledged.

REFERENCES

1. I. O. Bohachevsky, "Scaling of Reactor Cavity Wall Loads and Stresses," Los Alamos Scientific Laboratory report LA-7014-MS (November 1977).
2. T. G. Frank, I. O. Bohachevsky, L. A. Booth, and J. H. Pendergrass, "Heat Transfer Problems Associated with Laser Fusion," Proc. 16th Natl. Heat Transfer Conf., St. Louis, MO (August 1976).
3. R. W. Conn, et al., "Solase, a Conceptual Laser Fusion Reactor Design," University of Wisconsin report UWFDM-220 (December 1977).
4. I. O. Bohachevsky and J. F. Hafer, "Sputtering Erosion of Fusion Reactor Cavity Walls," Los Alamos Scientific Laboratory report LA-6633-MS (December 1976).
5. I. O. Bohachevsky and J. F. Hafer, "Dependence of Sputtering Erosion on Fuel Pellet Characteristics," Los Alamos Scientific Laboratory report LA-6991-MS (November 1977).
6. E. Stark, compiler, "Laser Fusion Program Progress Report," LA-6510-PR (November 1976), 116-8.
7. T. Frank, D. Freiwald, T. Merson, and J. Devaney, "A Laser Fusion Reactor Concept Utilizing Magnetic Filds for Cavity Wall Protection," Proc. 1st Topical Meeting on the Technology of Controlled Nuclear Fusion, San Diego, CA (1974).
8. J. C. Goldstein, I. O. Bohachevsky, and D. O. Dickman, "Ion Motion in Laser Fusion Reactor Studies," Bull. Am. Phys. Soc. 11, 21, 1186 (October 1976).
9. D. A. Freiwald and R. A. Axford, "Approximate Spherical Blast Theory Including Source Mass," J. Appl. Phys. 46, 1171-1174 (March 1975).
10. D. B. Henderson, "Pulse Unfocusing within Laser-Fusion Reactors," Nucl. Eng. and Design, 30, 111-116 (1974).
11. M. P. Hacker, D. R. Cohn, and B. Lax, Appl. Phys. Lett. 23, 392 (1973).
12. S. L. Thompson and H. S. Lawson, "Improvements in the CHART D Radiation Hydrodynamics Code II; A Revised Program," Sandia Laboratories report SC-RR-710713 (February 1972).